9-16-2019

Gamma-Ray Bursts Induced by Turbulent Reconnection

A. Lazarian
University of Wisconsin, lazarian@astro.wisc.edu

Bing Zhang
University of Nevada, Las Vegas, bing.zhang@unlv.edu

Siyao Xu
University of Wisconsin

Repository Citation

Lazarian, A., Zhang, B., Xu, S. (2019). Gamma-Ray Bursts Induced by Turbulent Reconnection. *Astrophysical Journal, 882*(2), 1-11. American Astronomical Society.
http://dx.doi.org/10.3847/1538-4357/ab2b38

The Astrophysical Journal, 882:184 (11pp), 2019 September 10 https://doi.org/10.3847/1538-4357/ab2b38

Gamma-Ray Bursts Induced by Turbulent Reconnection

A. Lazarian[1], Bing Zhang[2], and Siyao Xu[1,3]
[1] Department of Astronomy, University of Wisconsin, 475 North Charter Street, Madison, WI 53706, USA; lazarian@astro.wisc.edu, sxu93@wisc.edu
[2] Department of Physics and Astronomy, University of Nevada Las Vegas, NV 89154, USA; zhang@physics.unlv.edu
Received 2018 January 15; revised 2019 June 16; accepted 2019 June 18; published 2019 September 16

Abstract

We revisit the Internal-Collision-induced MAgnetic Reconnection and Turbulence model of gamma-ray bursts (GRBs) in view of the advances made in understanding of both relativistic magnetic turbulence and relativistic turbulent magnetic reconnection. We identify the kink instability as the most natural way of changing the magnetic configuration to release the magnetic free energy through magnetic reconnection, as well as driving turbulence that enables fast turbulent reconnection. We show that this double role of the kink instability is important for explaining the prompt emission of GRBs. Our study confirms the critical role that turbulence plays in boosting reconnection efficiency in GRBs and suggests that the GRB phenomena can be modeled in the magnetohydrodynamics approximation. That is, the modeling is not constrained by reproducing the detailed microphysical properties of relativistic magnetized plasmas.

Key words: gamma-ray burst: general – magnetic reconnection – turbulence

1. Introduction

Gamma-ray bursts (GRBs) are the most energetic phenomena in the modern universe. The physical mechanism that produces the observed γ-ray emission is still not identified (e.g., Kumar & Zhang 2015 for a recent review). Here we consider a scenario in which the magnetic reconnection in turbulent media induces GRBs. We employ the Lazarian & Vishniac (1999); henceforth LV99) model of reconnection, which has recently been extended for the relativistic regime (Takamoto et al. 2015; Takamoto 2018). This model proposes that the reconnection rate depends on the intensity of the surrounding turbulence.

In the standard fireball model (Paczýnski 1986; Goodman 1986; Shemi & Piran 1990; Rees & Mészáros 1992, 1994; Mészáros & Rees 1993, 1997, 2000), magnetic fields are not dynamically important, i.e., $\sigma \ll 1$ in the emission region, where σ is the ratio between the Poynting flux and the matter (baryonic + leptonic) flux. As an alternative picture that is becoming more and more popular, the magnetic field is dynamically important in GRB outflows, i.e., $\sigma_0 \gg 1$ at the central engine, and $\sigma \geqslant 1$ in the emission region (see, e.g., Usov 1992; Thompson 1994; Lazarian et al. 2003; Lyutikov & Blandford 2003; Zhang & Yan 2011, henceforth ZY11). In these models, the GRB emission is powered by the magnetic energy dissipation within the ejecta. Evidence supporting a Poynting-flux-dominated outflow in at least some GRB jets includes the lack of an observed weak thermal component in most GRB spectra (Zhang & Pe'er 2009); strongly polarized GRB emission (Coburn & Boggs 2003; Willis et al. 2005; Yonetoku et al. 2011, 2012; Zhang et al. 2019) and early optical emission (Steele et al. 2009; Mundell et al. 2013; Troja et al. 2017); an increasingly stringent upper limit of high-energy neutrino emission from GRBs (Zhang & Kumar 2013; Aartsen et al. 2015, 2016, 2017); and evidence of bulk acceleration or anisotropic emission in GRB prompt emission and X-ray flares (Jia et al. 2016; Uhm & Zhang 2016a, 2016b; Geng et al. 2017). A natural mechanism to dissipate magnetic energy is through magnetic reconnection.

Magnetic reconnection has been widely discussed as the energy dissipation mechanism for GRBs (see Lyutikov & Lazarian 2013 for a review and references therein). The reconnection in relativistic Pointing-dominated plasmas has been studied intensively in 2D configurations (see Lyutikov 2003; Lyutikov & Uzdensky 2003; Lyubarsky 2005; Takamoto 2013). Initially, the Petschek-type X-point configurations in collisionless media were studied. Later, when the limitations of this approach became obvious, studies of 2D plasmoid chain configurations induced by tearing became the focus of research efforts. However, a recent 3D relativistic reconnection study by Takamoto (2018) convincingly showed that the plasmoid reconnection is a feature related to 2D reconnection, while in 3D, it is turbulence that makes the reconnection fast. This work is in line with earlier studies of 3D self-driven nonrelativistic reconnection, where instead of plasmoids, turbulence was shown to play the dominant role (Oishi et al. 2015; Beresnyak 2017; Kowal et al. 2017).

Incidentally, these developments indicating the dominant role of turbulent reconnection are in line with the Internal-Collision-induced MAgnetic Reconnection and Turbulence (ICMART) model of GRBs proposed by Zhang & Yan (2011; henceforth ZY11). The model makes use of the theory of turbulent reconnection by LV99, which was earlier discussed in the framework of GRBs in Lazarian et al. (2003). However, the latter paper presented just an idea, while it was ZY11 who provided the quantitative study as well as the comparison of the predictions with available observations.

The ICMART model was shown to overcome several difficulties of the traditional internal shock model (Rees & Mészáros 1994; Kobayashi et al. 1997; Daigne & Mochkovitch 1998; Ghisellini et al. 2000; Kumar & McMahon 2008) and can well interpret the light curves and spectra of GRBs (Uhm & Zhang 2014; Zhang & Zhang 2014; Xu & Zhang 2017; Xu et al. 2018). It has made a deep impact on the GRB research.

However, eight years after the introduction of the ICMART model, we feel that it is time to revisit the problem and improve the model. For instance, it is advantageous to specify a natural

[3] Hubble Fellow.

mechanism for providing the magnetic field reversals for triggering magnetic reconnection within the model. We identify the kink instability as such a mechanism. As the main difference of this model from other kink-driven models of GRBs (e.g., Drenkhahn & Spruit 2002; Giannios & Spruit 2006; Giannios 2008; McKinney & Uzdensky 2012), the kink instability also induces turbulence (Galsgaard & Nordlund 1997; Gerrard & Hood 2003), which drives fast magnetic reconnection similar to the original model of ZY11.

In addition, at the time of the introduction of the ICMART model, the LV99 theory of turbulent reconnection was tested only by nonrelativistic simulations of reconnection in the presence of externally driven turbulence (Kowal et al. 2009). There were many uncertainties related to the application of the LV99 model to relativistic plasmas. The situation has changed recently. In particular, simulations of relativistic magnetohydrodynamics (MHD) turbulence (Takamoto & Lazarian 2016, 2017) modified our understanding of this process. In addition, relativistic simulations of turbulent reconnection have been performed, and they showed important differences from their nonrelativistic counterparts (Takamoto et al. 2015, henceforth TIL15).

We believe that our paper is timely as it not only considers a new way of triggering ICMART events, but also provides significant evidence in support of the turbulent reconnection that drives such events. This evidence comes from both theoretical and numerical studies that appeared after the ZY11 paper was published. In particular, the support of the turbulent reconnection in the relativistic regime, which is relevant to GRBs, has been obtained only recently. In what follows, we present the physical ingredients of our model in Section 2. We compare our model with GRB observations in Section 3. A discussion and conclusions of our results are provided in Sections 4 and 5.

2. Model Ingredients

2.1. A Brief Review of the ICMART Model

The pioneering model on GRBs built upon the turbulent reconnection is the ICMART model by ZY11. ZY11 speculated that the magnetic field reversals required to trigger ICMART events may be achieved through internal collisions among high-σ blobs. Under the framework of a helical magnetic configuration, they suggested that repeated collisions may accumulate magnetic distortions and eventually reach the threshold to trigger the runaway turbulent reconnection. In other words, ZY11 invokes collision-induced magnetic reconnection and turbulence to interpret GRB prompt emission. Deng et al. (2015) performed a series of relativistic MHD numerical simulations of collisions of high-σ magnetic blobs. They found that significant magnetic dissipation can indeed occur with an efficiency above 30%, which agrees with the analytical estimate of ZY11. The simulations also showed the existence of local Doppler-boosted regions due to reconnection, which are consistent with the mini-jets invoked in magnetic dissipation models of GRBs (Lyutikov & Blandford 2003) and shape the light curves of GRBs (Zhang & Zhang 2014). The model entails a relatively large emission radius from the central engine and has a list of features that match the observations very well (see Section 3 below).

It is important to point out that local magnetic field reversals induced by turbulence are not adequate in releasing the free energy stored in large-scale helical magnetic fields. A triggering mechanism to change the magnetic field configuration is necessary to create large-scale magnetic field reversals ready for the release of magnetic free energy. In this paper, we introduce the kink instability as the key element of this triggering mechanism.

Our present model is constructed based on the ICMART model and thus shares some common features with it that were described in detail in ZY11. Here we only focus on the theoretical modifications and discuss their necessity and significance. As one of the main differences from the original ICMART model, we introduce a more favorable mechanism of initiating magnetic reconnection. As mentioned above, instead of collisions of magnetized slabs adopted in the ICMART model, we employ the kink instability, which naturally takes place in the relativistic and strongly magnetized jet of a GRB and leads to a change in magnetic field configuration (see Section 2.2). The development of kink instability in a relativistic and Poynting-dominated jet has been shown in numerical simulations (Mizuno et al. 2012, 2014a, 2014b; O'Neill et al. 2012; Singh et al. 2016; Alves et al. 2018). In addition, as the theoretical core of both the ICMART model and our current model, turbulent reconnection theory has been extended to relativistic regime. The ICMART model was built upon the theory of nonrelativistic turbulent reconnection. Now with new theoretical understanding and numerical tests (e.g., Takamoto et al. 2015) on relativistic turbulence and relativistic turbulent reconnection, we can construct a model on more solid foundations.

2.2. Triggering Magnetic Reconnection through Kink Instability

Both theoretical arguments and observational evidence suggest that GRBs originate from ultrarelativistic jets with bulk Lorentz factor $\Gamma > 100$ (e.g., Lithwick & Sari 2001; Taylor et al. 2004; Zhang et al. 2006; Kato et al. 2008; Abdo et al. 2009a, 2009b). Various polarization studies of prompt and afterglow emission indicate the presence of a large-scale ordered magnetic field in the ejecta (Yonetoku et al. 2011, 2012; Mundell et al. 2013; Wiersema et al. 2014). Rotation is a generic property of astrophysical jets that arises from the transfer of the angular momentum from the accreting material and the central engine through the magnetic field (see Blandford & Znajek 1977; Blandford & Payne 1982; Bisnovatyi-Kogan & Lovelace 2001). Such a rotation is expected to produce a magnetic spiral within the jet associated with a GRB (see more in Kumar & Zhang 2015). Although a magnetic spiral has substantial free magnetic energy, it does not reconnect on its own because the magnetic fields in adjacent magnetic coils are of the same direction. Therefore, the spiral should be destabilized to allow for the magnetic reconnection.

A kink instability is one of the plausible processes that can destabilize the spiral magnetic field in a jet. The stability of current-carrying force-free (or nearly force-free) fields has been extensively studied for a cylindrical geometry in the astrophysical context (see Baty & Heyvaerts 1996; Li 2000; Baty 2001; Gerrard et al. 2002; Török et al. 2004). Physically, the kink instability arises as the winding of the magnetic field in a jet becomes so tight that a particular threshold is exceeded.

This process can be induced if, for instance, the jet is slowed down by external media, or there are variations of velocity and density within the jet. As this happens, the adjacent coils of magnetic fields become tighter, and subsequently the kink instability develops. This process is easy to understand: the closer the coils, the more energy is stored in winding the coil. Therefore it becomes energetically advantageous to change the magnetic field configuration through the kink. More details on triggering kink instability in different scenarios are provided in Section 2.2.2. While in the coil the adjacent magnetic fields are parallel and cannot reconnect, the new configuration formed by the kink instability contains field reversals and therefore is prone to reconnection. As a result, oppositely directed magnetic fluxes can reconnect, releasing the stored magnetic free energy.

2.2.1. Conditions for Kink Instability

For simplicity, let us consider a cylindrical jet with a length L and a cross-section radius R. In the case of a helical magnetic field geometry, the spiral magnetic field obeys

$$\frac{Rd\theta}{dz} = \frac{B_t}{B_p}, \tag{1}$$

where B_p and B_t are the poloidal and toroidal magnetic field strengths, respectively. θ gives the toroidal direction, and z is the distance along the jet axis. One can then define a safety factor q, so that $2\pi R/qL = B_t/B_p$ is satisfied. The kink instability condition is given by

$$q = \frac{2\pi RB_p}{LB_t} < 1, \tag{2}$$

which is called the Kruskal–Shafranov (KS) criterion. This can be rewritten as

$$\frac{B_t}{B_p} > \frac{2\pi R}{L}. \tag{3}$$

The growth rate of the instability is $\gamma_g \sim \frac{B}{\rho R}\sqrt{(1/q)(1/q-1)}$ (see more descriptions in Goedbloed & Poedts 2004). It grows faster for a stronger magnetic field $B \sim B_t$ (for a toroidally dominated field) and a lower plasma density ρ.

The above idealized criterion only applies to the situation with a constant ρ and uniform winding of magnetic fields. It should be modified in realistic settings of GRBs with a more complex structure of density and magnetic fields. In addition, in the relativistic case, it is appropriate to adopt the force-free approximation where only the charges, currents, and fields are accounted for, but the inertia and pressure of the plasma are ignored. By taking into account the stabilizing effect of the rotating magnetic spiral, one can extend the classical KS criterion. Under this consideration, we find that the kink instability arises if both the KS criterion and an additional condition (Tomimatsu et al. 2001)

$$\frac{B_t}{B_p} > \frac{R}{R_{\rm LC}} = \frac{R\Omega_B}{c} \tag{4}$$

are satisfied. Here c is the speed of light, Ω_B is the angular velocity of the magnetosphere of the central engine, which is also the angular velocity of the spiral magnetic field, and $R_{\rm LC} = c/\Omega_B$ is the radius of the light cylinder of the central engine. For GRBs, $L = c\Delta t_{\rm slow} = 3 \times 10^{10}$ cm$(\Delta t_{\rm slow})$, where $\Delta t_{\rm slow}$ is the typical duration of the "slow variability component" of GRB light curves, which defines the duration of central engine activity for each active episode of GRB emission (Gao et al. 2012; Xu & Li 2014). The central engines of GRBs are typically millisecond rotators, so that $R_{\rm LC} = 4.8 \times 10^6$ cmP_{-3}, where P_{-3} is period in units of 10^{-3} seconds or milliseconds. As a result, the criterion Equation (4) is more stringent than Equation (3), and thus it is more relevant.

More complicated setups for the development of kink instability within relativistic jets have been explored numerically (see McKinney & Blandford 2009; Mizuno et al. 2009, 2011a, 2011b, 2012, 2014a, 2014b; Mignone et al. 2010; O'Neill et al. 2012). These simulations revealed a variety of initial conditions that influence the detailed growth and evolution of kink instability. The numerical results are consistent with the above general conditions in Equations (3) and (4), which we use as a guidance for our further discussion.

For a Kerr black hole as the central engine that launches a relativistic jet, the jet is kink stable if the condition

$$|\Omega_B - \Omega_{\rm BH}| < \Omega_B \tag{5}$$

is satisfied (Tomimatsu et al. 2001). This requires that the magnetosphere angular velocity does not significantly differ from the black hole angular velocity, that is (Tomimatsu et al. 2001),

$$\Omega_B \geqslant \Omega_{\rm BH}/2. \tag{6}$$

Such a condition is usually satisfied for a GRB engine, so that for a helical jet launched from a hyper-accreting BH, the jet may propagate to a large distance without triggering kink instability.

2.2.2. Triggering Kink Instability

For a steady cylindrical jet, from Equation (4) one can see that the kink instability condition is either satisfied or not throughout the jet propagation. Such a conclusion applies even in a more general case with the jet radius evolving with the distance r from the central engine. Without losing generality, one can write

$$R \propto r^b, \tag{7}$$

where $0 \leqslant b \leqslant 1$, with $b = 0$ and $b = 1$ corresponding to a cylindrical and a conical jet, respectively. The conservation of magnetic flux gives

$$B_p \propto R^{-2} \propto r^{-2b}, \tag{8}$$

$$B_t \propto R^{-1} \propto r^{-b}. \tag{9}$$

This suggests that both sides in Equation (4) are proportional to r^b, so that Equation (4) is satisfied (or not) throughout the jet regardless of the geometrical configuration of the jet. Therefore, in order to trigger kink instability in a jet, additional mechanism is needed to alter the magnetic configuration of the jet.

There are at least three possible ways of triggering kink instability in the GRB context. In the first scenario, a magnetized jet is decelerated as it penetrates the stellar envelope of the progenitor star. This would induce significant magnetic energy dissipation below the photosphere and result in a matter-dominated fireball with strong photospheric emission. It more likely happens during the early phase of a

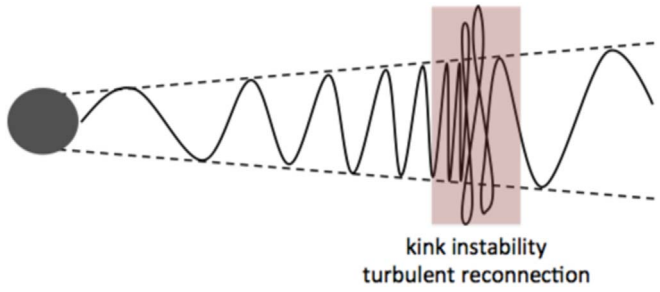

Figure 1. Illustration of the kink instability in the GRB jet.

GRB. At later times after the early portion of the jet successfully escapes the star, the Poynting-flux-dominated jet is able to reach a large distance from the central engine before significant dissipation happens. The second scenario to trigger kink instability involves external pressure from the ambient medium. Analogous to the external shock model of GRBs (Rees & Mészáros 1992; Mészáros & Rees 1993, 1997), it invokes external medium to decelerate the jet and thus the increase of the B_t/B_p ratio in the jet, which triggers kink instability. The emission region of this model is close to the deceleration radius, i.e., $R_{\rm GRB} \sim R_{\rm dec} \sim 10^{17}$ cm for typical GRB parameters. The third scenario, similar to the internal shock model (Rees & Mészáros 1994) and the ICMART model (ZY11) of GRBs, requires intrinsic irregularity of the central engine and interactions between different parts in the jet with different bulk Lorentz factors to increase the B_t/B_p ratio and trigger kink instability. As illustrated in Figure 1, due to the velocity variations within the strongly magnetized jet launched by the central engine, the faster part of the jet approaches its slower part in front, where the spiral magnetic field is squeezed together and the condition for triggering the kink instability (see Equation (4)) is satisfied. The resulting magnetic flux reversals entail magnetic reconnection. In the presence of turbulence, it is substantially efficient in energy dissipation to account for the GRB emission (see Section 2.3).

The third scenario is more consistent with the GRB observational data (see Section 3 for more discussions). Similar to the ICMART model (ZY11), the emission radius in this scenario is $R_{\rm GRB} \sim \Gamma^2 c\Delta t_{\rm slow} \sim 10^{15}$ cm. This can be understood based on the following reasons. In the ICMART model, the collision of two magnetized shells is responsible for altering the magnetic configuration and triggering reconnection. In the current scenario, instead of the collision of two physically separated magnetized shells, it simply requires a continuous jet with velocity fluctuations within it. The trailing high-Γ part of the jet catches up with the leading low-Γ part at a radius similar to the case of collisions. Without a direct collision, the ram pressure of the trailing part squeezes the magnetic field configuration in the system, leading to the onset of kink instability and magnetic reconnection. A GRB is then produced around the same radius as the ICMART model. It is important to note that kink instability does not necessarily disrupt the jet, but only results in the change of magnetic field structure, which enables the subsequent magnetic reconnection. Magnetic reconnection is driven by the free energy of magnetic fields. In a generic situation of 3D geometry, it causes the annihilation of contacting oppositely directed magnetic fluxes.

Relativistic ideal MHD simulations that revealed kink instability and indicated turbulent reconnection in a jet have been performed by Singh et al. (2016). They found that the kink instability naturally develops in the jet and the kink-unstable regions are associated with the magnetic reconnection. Due to the limited numerical resolution, the confirmation of turbulent reconnection was not possible in Singh et al. (2016). We note, however, that unlike numerical simulations, turbulence is inevitable in high-Reynolds number (*Re*) astrophysical jets (see 2.4). In view of this, we believe that these simulations provide numerical evidence for our theoretical model.

2.3. Reconnection of Relativistic Turbulent Magnetic Fields

The typical value of *Re* in GRB conditions is $Re \sim (10^{27}$–$10^{28}) \gg 1$ (ZY11), and therefore the ICMART model took the turbulence into account appealing to the turbulent reconnection as the main driver of the conversion of magnetic energy. Indeed, at such a high *Re*, turbulence is inevitable. The kink instability in the high-*Re* magnetized plasma is expected to induce turbulence. Thus the magnetic reconnection triggered by the kink instability takes place in a turbulent environment.

We provide a concise description of the LV99 theory of nonrelativistic turbulent reconnection in the Appendix. The LV99 model was employed by ZY11 within the ICMART scenario. For GRBs, we deal with relativistic plasmas with strong magnetization $\sigma \equiv B^2/4\pi\rho h c^2 \gg 1$, where $h = 1 + 4(p/\rho c^2)$ is the specific enthalpy of relativistic ideal gas, and ρ, p, and c are mass density, pressure, and speed of light, respectively. Therefore the application of LV99 model of nonrelativistic turbulent reconnection should be subjected to scrutiny.

First of all, direct application of the Goldreich-Sridhar (1995; henceforth GS95) model for nonrelativistic Alfvénic turbulence, which is at the core of the LV99 model of turbulent reconnection, must be reconsidered. The GS95 model has its counterpart for relativistic Alfvénic turbulence (Thompson & Blaes 1998). This relativistic analog of the GS95 model was supported by numerical simulations in the case of decaying turbulence by Cho (2005) under the so-called force-free approximation.[4] Although the subsequent simulations of fully relativistic MHD turbulence (Zhang et al. 2009; Beckwith & Stone 2011; Inoue et al. 2011; Mizuno et al. 2011a, 2011b, 2014a, 2014b; Zrake & MacFadyen 2012, 2013; Garrison & Nguyen 2016) delivered results roughly consistent with the GS95 expectations, more recent numerical studies by Takamoto & Lazarian (2016, 2017) revealed important differences between the relativistic and nonrelativistic compressible MHD turbulence (see Cho & Lazarian 2002, 2003; Kowal & Lazarian 2010). In particular, while the scalings of Alfvén and slow modes were shown to be similar to those in the nonrelativistic case, the coupling of Alfvén and fast modes was demonstrated to be significantly stronger in the relativistic case. This difference is important for determining the reconnection efficiency in relativistic compressible MHD turbulence.

In the LV99 model, the thickness of outflow region Δ is determined by the magnetic field wandering, which is induced by the Alfvénic component of compressible turbulence (see the Appendix and the discussion on decomposing MHD turbulence into fast, slow, and Alfvénic components in Cho & Lazarian 2003). In comparison, the increase of the outflow region induced by the fast and slow components of MHD turbulence can be neglected. In the corresponding LV99 expression of Δ,

[4] In relativistic MHD turbulence, the force-free approximation corresponds to the zeroth term of expansion of relativistic MHD over a small parameter $1/\sigma$.

one should use only the energy associated with the Alfvénic cascade:

$$\Delta \approx L_x\left(\frac{\epsilon_{\rm inj,Alf} l}{c_{\rm A}^3}\right)^{1/2} \min\left[\left(\frac{L_x}{l}\right)^{1/2}, \left(\frac{l}{L_x}\right)^{1/2}\right], \quad (10)$$

where we modified Equation (16) by using $c_{\rm A}$, which is the Alfvén speed in relativistic environment. Other notations include the injection scale l and the longitudinal extent of the outflow region L_x. We also used the notation for the energy cascade rate $\epsilon_{\rm inj,Alf}$, corresponding to the Alfvénic component of the MHD turbulent cascade that is responsible for the broadening of the outflow region. In other words, $\epsilon_{\rm inj,Alf} \approx \epsilon_{\rm inj} - \epsilon_{\rm slow} - \epsilon_{\rm fast}$, where $\epsilon_{\rm inj}$, $\epsilon_{\rm fast}$, and $\epsilon_{\rm slow}$ are the cascade rates corresponding to the total injected turbulent energy, and the fast and slow components of the turbulent energy. The above relation is only approximate due to the increased coupling of fast and Alfvén modes. In addition, compared to Equation (16), we disregard a factor of $\sqrt{2}$, which in any case cannot be defined using scaling arguments.

As we discuss in the Appendix, $\epsilon_{\rm inj}^{1/2}$ is proportional to the injection velocity $V_{\rm inj}$. To be consistent with numerical simulations in Takamoto et al. (2015; henceforth TIL15), one can perform the expansion over $V_{\rm inj}/c_{\rm A}$, which amounts to substituting

$$\left(\frac{\epsilon_{\rm inj,Alf} l}{c_{\rm A}^3}\right)^{1/2} \approx \left(\frac{\epsilon_{\rm inj} l}{c_{\rm A}^3}\right)^{1/2} - \alpha\left(\frac{\epsilon_{\rm inj} l}{c_{\rm A}^3}\right), \quad (11)$$

where the coefficient α is on the order of unity, as suggested by the numerical results in TIL15. This is also consistent with later studies on the energy cascade of relativistic MHD turbulence and the transfer of energy to compressible motions (Takamoto & Lazarian 2016, 2017).[5]

Another important difference of the reconnection model that was adopted in the original version of the ICMART model and our present version is the effects of compressibility. The change of the plasma density comes from the mass conservation constraint. In the continuity equation given by Equation (17), the difference between the plasma density far from the reconnection sheet ρ_i and that in the outflow region ρ_s is significant. Moreover, it is easy to see that the ratio of the two densities is expected to depend on the turbulent injection rate. In the absence of cooling, the loss of energy in the system is expected due to the outflow of plasmas from the reconnection layer. Therefore, according to Equations (10) and (11), the outflow of energy from the system is roughly proportional to $\epsilon_{\rm inj}^{1/2}$. The heating is naturally proportional to $\epsilon_{\rm inj}$. This causes the readjustments in the system dynamics, and as a result of heating, the plasma density decreases, which decreases the reconnection rate. The corresponding change of density was derived in TIL15 and within the accepted notations can be presented as

$$\frac{\rho_s}{\rho_i} \approx 1 - \chi\left(\frac{\epsilon_{\rm inj} l}{c_{\rm A}^3}\right)^{\frac{1}{2}}, \quad (12)$$

where χ is a function of σ, and l is the injection scale of turbulence. The validity of Equation (12) was confirmed numerically in TIL15.

Under the above considerations, the corresponding expression of the turbulent reconnection velocity can be written as

$$V_{\rm rec,relativ.} \approx c_{\rm A}\left(\frac{\rho_s}{\rho_i}\right)\left(\frac{\epsilon_{\rm inj,Alf} l}{c_{\rm A}^3}\right)^{1/2} \times \min\left[\left(\frac{L_x}{l}\right)^{1/2}, \left(\frac{l}{L_x}\right)^{1/2}\right], \quad (13)$$

where Equations (11) and (12) should be substituted to express the injection rate for the Alfvénic cascade and the density ratio, respectively. Unlike the original expression in LV99, Equation (13) predicts the decrease of the reconnection efficiency with the increase of turbulent energy input. Nevertheless, the observed reconnection rates in TIL15 simulations are fast, e.g., $V_{\rm rec,relativ} \sim 0.05 c_{\rm A}$, and comparable with the relativistic Petschek reconnection rate reported in, e.g., Lyubarsky (2005). The injection scale l in the simulations by TIL15 was $1/16 L_x$, and thus the corresponding factor in Equation (13) is $1/4$. The evaluation of of the expression $\left(\frac{2\alpha\epsilon_{\rm inj,Alf} l}{c_{\rm A}^3}\right)^{1/2}$ is somewhat uncertain in the case of kink instability. Instead, we follow TIL15 and substitute this expression by the ratio $V_{\rm inj}/c_{\rm A}$. For the highest value of $\sigma = 5$ adopted by TIL15, there is $V_{\rm rec,relativ.} \sim 0.03 c_{\rm A}$ for $V_{\rm inj}/c_{\rm A} = 0.5$. Extrapolating these values to the injection scale $l \sim L_x$ as expected for the case of kink instability, one obtains $V_{\rm rec,relativ} \sim 0.06 c_{\rm A}$. This value of the reconnection rate should be considered as a lower limit for the reconnection process in GRBs because the cooling of plasmas would increase the ρ_s/ρ_i ratio and thus increase the resulting reconnection rate. The detailed study of the cooling effects will be done elsewhere, but within the present paper it is important to remark that our estimate that follows from Equation (13) does not differ much from the rate $V_{\rm rec,relativ.} \sim 0.1 c_{\rm A}$ that was used in the ICMART model on the basis of the analysis of the nonrelativistic isothermal simulations in Kowal et al. (2009; see also Zhang & Zhang 2014 for the discussion on the spectral curves of prompt emission).

2.4. Driving of Turbulence and Turbulent Reconnection

The theoretical picture in LV99 suggests that turbulence can be enhanced by reconnection. Consider a magnetically dominated low-β plasma with weakly turbulent magnetic flux tubes coming into contact with each other, where β is the ratio of gas pressure to the magnetic pressure. Initially, the magnetic reconnection proceeds at a slow pace, as magnetic field lines are nearly laminar and the ratio of outflow region Δ to L_x is very low. With the increase of Δ, when Re of the outflow becomes considerably higher than unity (see Equation (14)), the rising turbulence in the outflow will increase the

[5] We note that the incompressible part of slow modes does not contribute to widening of the outflow region. As a result, we do not expect to observe any strong dependence of the reconnection rate on $\sqrt{\sigma}$ that is expected if the decrease of reconnection efficiency were only due to the transfer of energy from Alfvén to fast modes. This dependence was not observed in the TIL15 simulations.

surrounding magnetic fluctuations, inducing the higher level of field line wandering. This further extends the width of the outflow region Δ and increases the reconnection rate, as well as the energy injection in the system. A higher level of energy injection and a higher *Re* of the outflow both enhance the level of turbulence in the system.

The above positive feedback can additionally enhance the level of turbulence that is initially excited by the kink instability, and leads to an explosion of reconnection. A quantitative model for such a process was presented for a nonrelativistic plasma with dominant magnetic pressure (low-β plasma) in Lazarian & Vishniac (2009).[6]

In addition to being driven by kink instability, reconnection also serves as a source of turbulence. Recently a number of groups performed 3D reconnection simulations with no turbulence in the initial setup. In these simulations the development of MHD turbulence as a result of reconnection in both compressible and incompressible media was reported (see Oishi et al. 2015; Huang & Bhattacharjee 2016; Beresnyak 2017; Kowal et al. 2017). A more quantitative study by Kowal et al. (2017) showed that the GS95 turbulence is generated as a result of reconnection and the LV99-type reconnection ensues. These simulations were performed in a nonrelativistic regime, and in addition, the transfer from tearing reconnection to a fully turbulent reconnection was indicated from relativistic simulations of a pulsar wind in Zrake (2016). There it was found that the magnetic energy dissipation rate is insensitive to the grid resolution, showing that the reconnection in the presence of turbulence is universal with respect to the unresolved physics. Relativistic MHD simulations by Takamoto (2018) also showed the evolution of reconnection in a 3D setup and the transfer to relativistic turbulent reconnection.

It is important to stress that the bursty character of turbulent reconnection observed in both nonrelativistic and relativistic reconnection simulations can account for the erratic behavior of GRB emission (see Section 3).

3. Comparison with Observations

The GRB prompt emission model outlined here shares many properties with the ICMART model and has the advantage of interpreting the observational data of at least some GRBs. In this section, we summarize how this model compares many observational properties of GRBs (see also Section 9.10 of Zhang (2018) for a more detailed discussion):

1. Light curves: Observationally, GRB light curves are irregular and variable. Studies show that the light curves can be often decomposed into multiple "pulses" (Norris et al. 2005), each with durations of seconds. On the other hand, bursts can have rapid variability on a timescale as short as milliseconds. These "fast" spiky peaks often overlap with the "slow" pulse component (Gao et al. 2012; Xu & Li 2014). Similar to the ICMART model (ZY11), our kink-triggered GRB model interprets the slow pulses as individual kink-triggered events, while the fast spikes are interpreted as due to comoving-frame mini-jets produced by turbulent reconnection of individual units in a moderate-σ jet. Monte Carlo simulations have shown that such a model can reproduce a variety of observed GRB light curves (Zhang & Zhang 2014). Similarly, Giannios et al. (2009) suggested that the jets in a Poynting flux-dominated jet powered by magnetic dissipation through reconnection can account for the fast TeV variability observed in blazars.
2. Spectra: Observationally, GRB spectra have a dominant "Band-function" component (Band et al. 1993) with a typical low-energy spectral index $\alpha \sim -1$ (Preece et al. 2000; Nava et al. 2011; Zhang et al. 2011). Some bursts have a very hard spectral index ($\alpha > -2/3$), which is beyond the limit of the so-called synchrotron line-of-death (Preece et al. 2000). In these cases, the spectra are likely of a thermal origin, which is consistent with emission from a fireball photosphere (Mészáros & Rees 2000; Lazzati & Begelman 2010). Observationally, thermally dominated GRBs have been observed (Abdo et al. 2009b; Ryde et al. 2010; Pe'er et al. 2012), but for the majority of the GRBs, the thermal component is either subdominant (Guiriec et al. 2010; Axelsson et al. 2011) or not detectable (Abdo et al. 2009a; Zhang et al. 2016; Burgess et al. 2018). This suggests that the GRB jets are Poynting flux dominated at the central engine, and likely in the emission region as well (Zhang & Pe'er 2009; Gao & Zhang 2015). For these GRBs, the Band component is likely of a synchrotron radiation origin. Because photosphere emission is suppressed in these bursts, particles are likely accelerated in the turbulent reconnection region, rather than from internal shocks. At a large radius (beyond 10^{15} cm) from the central engine, the magnetic field strength is low enough so that synchrotron cooling is no longer in the deep fast-cooling regime. As the jet streams outward, it is likely that the comoving magnetic field strength continuously decreases with time. A fast-cooling synchrotron spectrum in this model would deviate from the standard $\alpha = -3/2$ prediction, and give rise to a harder spectrum with $\alpha \sim -1$ (Uhm & Zhang 2014; Geng et al. 2018). Due to turbulent acceleration of electrons, the balance between cooling and acceleration of electrons would lead to a typical electron spectral index $p = 1$, which gives rise to a photon power-law spectral index $\alpha \sim -1$ (Xu & Zhang 2017; Xu et al. 2018). Note that these two ways to interpret $\alpha = -1$ make use of the two important predictions of our model: the large radius needed to have a harder fast-cooling spectrum is consistent with requiring magnetized shells that interact to trigger kink instability, and turbulent acceleration needed to account for the $p = 1$ is the natural consequence of turbulent reconnection induced from kink events. One interesting prediction of the model is that kink is easy to develop early on with the existence of the progenitor stellar envelope so that a bright thermal component may develop in the early phase of a GRB. At later times, the jet would be Poynting flux dominated with emission powered by synchrotron radiation at a large emission radius. This is consistent with the recently observed bright multiepisode in GRB 160625B, which showed a transition from a fireball to Poynting-flux-dominated flow (Troja et al. 2017; Zhang et al. 2018).

[6] In addition to the application to GRB emission, this bootstrap turbulent reconnection can also explain the formation of solar flares, as their existence requires both phases of slow and fast reconnection. In addition, the turbulence generated from the reconnection in one region can also trigger the reconnection in surrounding regions (LV99). Such a process was reported in the observations of Sych et al. (2009, 2015; see also Gutiérrez et al. 2017).

3. Spectral lag and E_p evolution: The current picture invokes each kink event as one radiation unit. The observed broad pulse emission reflects the radiation history of the emission region as it streams outward, rather than the history of the central engine activity. Such a picture naturally accounts for the observed spectral lag behavior (Norris et al. 2000) and E_p evolution patterns (Lu et al. 2012), which is difficult to explain for the models invoking a small emission radius (Uhm & Zhang 2016a; Uhm et al. 2018).
4. Polarization: Polarized γ-ray emission has been claimed in some GRBs (Coburn & Boggs 2003; Willis et al. 2005; Yonetoku et al. 2011, 2012; Zhang et al. 2019). Even though with low significance, these observations nonetheless suggest that there is likely an ordered magnetic field component in the GRB emission region. This hypothesis is further supported by the detection of polarized optical emission shortly after γ-ray emission, either in the reverse-shock region (Steele et al. 2009; Mundell et al. 2013) or in the internal prompt emission region (Troja et al. 2017). Our model can naturally account for all these observations.
5. Neutrino upper limit: The IceCube Neutrino Observatory is placing progressively stringent upper limits on neutrino fluxes from GRBs (Aartsen et al. 2015, 2016, 2017), which greatly reduces the available parameter space of the models that invoke a small emission radius (e.g., the photosphere models and the internal shock models, Zhang & Kumar 2013). Because our kink-triggered magnetic dissipation model has a similar emission radius as that of ICMART, our model can comfortably satisfy the neutrino nondetection constraint.

4. Discussion

4.1. Justification for Turbulent Reconnection in GRBs

Other theories have been proposed for increasing the turbulent reconnection rate. Therefore, it is necessary to discuss why we believe that the turbulent reconnection is the most relevant process in the GRB context.

The model suggested by Petscheck (1964) was for decades the commonly accepted mechanism for fast magnetic reconnection. The 2D mechanism reached the apogee of popularity after numerical simulations including the Hall effect showed that the Petschek-type X-point reconnection can happen in a collisionless plasma (Shay et al. 1998; Drake 2001; Drake et al. 2006). However, as pointed out by, e.g., LV99, such configurations are very difficult to realize in realistic astrophysical settings. Indeed, supporting the X-point configuration in the presence of external forcing seems not natural. This was also confirmed in numerical simulations, which indicated that instabilities of the 2D so-called Y-type reconnection layer provide a more natural development of the 2D reconnection.

The 2D model for fast reconnection relies on the instabilities of the Sweet–Parker reconnection layer, e.g., tearing instability. Its importance was strongly advocated by Syrovatskii (see 1981 for a review and reference therein) and has been widely recognized by the community only more recently (Biskamp 1986; Shibata & Tanuma 2001; Daughton et al. 2006, 2009, 2011, 2014; Loureiro et al. 2007, 2012; Lapenta 2008; Bhattacharjee et al. 2009; Cassak et al. 2009; Huang & Bhattacharjee 2010, 2012, 2013; Shepherd & Cassak 2010; Uzdensky et al. 2010; Bárta et al. 2011; Huang et al. 2011; Shen et al. 2011; Fermo et al. 2012; Takamoto 2013; Wyper & Pontin 2014). The reconnection rates obtained in the MHD regime were limited to $\sim$0.01 of V_A (e.g., Loureiro et al. 2007), which is rather slow to account for the energy dissipation in GRBs. Most of the simulations of tearing reconnection have been carried out in 2D setups, and they do not involve turbulence.[7] Plasma effects can increase the rate of tearing 2D reconnection, but this does not answer the question of what is happening in 3D case.

The development of turbulence and the suppression of tearing instability were reported in a number of 3D numerical simulations (see Oishi et al. 2015; Beresnyak 2017; Kowal et al. 2017), including the first 3D simulations of relativistic reconnection with self-driven turbulence in Takamoto (2018). Furthermore, in Kowal et al. (2019, in preparation), the role of tearing instability in 3D simulations was subjected to further quantitative investigation. It is well known that turbulence can efficiently suppress the tearing instability (Somov & Verneta 1993). This was also numerically confirmed in reconnection simulations in Kowal et al. (2019, in preparation). All these results testify that the tearing reconnection may be important for the initial stage of reconnection process, if the medium is initially laminar. As turbulence develops, the turbulent reconnection takes over. From the general perspective, this is a natural process because in turbulent flows the flux freezing is not valid. Indeed, this violation of flux freezing in turbulent flows that follows from theory (LV99, Eyink 2010; Eyink et al. 2011) has been convincingly demonstrated by numerical simulations in Eyink et al. (2013). Recent simulations using the PIC code by H. Li (2019, private communications) and the simulations in high-Prandtl number media by Jafari et al. (2018) provide additional evidence that the turbulent reconnection is a robust process, which is unlikely to be derailed by plasma effects. This corresponds to the conclusions of the extensive theoretical study by Eyink (2015), where a generalized Ohm's law involving both turbulence and plasma effects was derived.

While the detailed discussion of why the tearing instability is subdominant or suppressed in 3D are beyond the scope of our paper (see Lazarian et al. 2015; Takamoto 2018), one can provide general arguments that even if initially the level of turbulence is low and tearing instabilities are dominant, the generic final picture of reconnection will be governed by turbulence. The relevant fast reconnection in astrophysics takes place at a very large Lundquist number, i.e., $S \gg 1$. This number is related to Re of the outflow $Re = \Delta V_A/\nu$, where ν is the viscosity, by

$$Re = S\frac{V_{\rm rec}}{V_A}Pt^{-1}, \tag{14}$$

where $Pt = \nu/\eta$ is the Prandtl number, and η is the ohmic resistivity. Thus for $V_{\rm rec}$ being 0.01 or a larger fraction of V_A, Re of the outflow increases in parallel with S. In the magnetic

[7] 2D and 3D MHD turbulence are different. The most important component of 3D MHD turbulence, the Alfvénic cascade (see Lithwick & Goldreich 2001, Cho & Lazarian 2003), is not present in 2D MHD turbulence. The magnetic field wandering induced by Alfvénic modes is the driver of the fast reconnection as described in LV99. Whether the reconnection is fast or slow in 2D MHD turbulence is a matter of debate, as discussed in Eyink et al. (2011). At the same time, it is numerically proven in Eyink et al. (2013) that 3D MHD turbulence violates the flux freezing, which is in agreement with the arguments in LV99.

dissipation region of GRBs with $\sigma > 1$, S is essentially the magnetic Reynolds number in the Bohm diffusion limit, which is $\sim 3 \times 10^{12}$ for typical GRB parameters (ZY11). In the Bohm diffusion approximation, η can be comparable to ν (ZY11), and thus Pt is on the order of unity. Therefore, it is natural to expect the outflow to be turbulent and the transfer to turbulent reconnection to occur (see Lapenta & Lazarian 2012).

All in all, while at the time of its introduction, the ICMART model had little support of having the turbulent reconnection as the driver of fast magnetic reconnection, more recent studies provide important evidence supporting the foundations of the model.

4.2. Comparison with Other GRB Models Based on Magnetic Reconnection

Several other GRB models exist that invoke magnetic reconnection as the origin of prompt emission. In the following we comment on how our model differs from these models.

Thompson (1994) envisaged a scenario of invoking mildly relativistic Alfvén turbulence excited in the wind by reconnection, or by hydrodynamical instabilities triggered by magnetic tension. The reconnection process was discussed within the framework of the Petschek (1964) mechanism, which was later found unstable and not confirmed by numerical simulations. A photon spectrum is formed via Comptonization of thermal photons at a moderate or high scattering optical depth. The resulting spectrum is quasi-thermal, and the emission radius is close to the central engine. This is the earliest version of magnetic dissipative photosphere model in the GRB literature. Many authors further developed the magnetic dissipative photosphere model by invoking magnetic reconnection below the photosphere (e.g., Drenkhahn & Spruit 2002; Giannios 2006; Veres et al. 2013; Beniamini & Giannios 2017). This model predicts a dominant photosphere emission component in the GRB prompt emission spectra, which may be consistent with some GRBs (e.g., GRB 090902B, Abdo et al. 2009b; Ryde et al. 2010; Pe'er et al. 2012), but may not explain those GRBs that do not show significant thermal emission component.

Spruit et al. (2001) discussed a striped-wind magnetic field configuration with alternating polarity and argued that magnetic reconnection can happen continuously in the outflow both below and above the photosphere. They assumed that reconnection can proceed rapidly with local Alfvén speed and argued that efficient γ-ray emission can be produced. The radiation spectrum was not calculated.

McKinney & Uzdensky (2012) proposed a reconnection switch model of GRBs. They argued that as the GRB jet streams out, the comoving density in the jet decreases steadily. At a certain distance from the central engine, magnetic reconnection switches from the collisional regime (associated with Sweet–Parker reconnection) to the collisionless regime (associated with Petscheck reconnection) so that the reconnection speed increases rapidly. Significant magnetic dissipation occurs and a GRB is triggered. The switching distance could be below or above the photosphere radius, and the authors emphasized the possible enhancement of photosphere emission. This enhancement is useful to interpret a (small) fraction of bursts. However, for the majority of GRBs, evidence suggests that the emission region is quite far away from the central engine (10^{15}–10^{16} cm). The model cannot hold on that long before rapid reconnection occurs.

5. Conclusions

This paper presents a further step in the development of the ICMART model. The original model in ZY11 pioneered the concept of turbulent magnetic reconnection for explaining major features of the GRB physics. The turbulent reconnection model that ZY11 appealed to was constructed in LV99, and it was tested with nonrelativistic 3D MHD simulations in Kowal et al. (2009). However, at the moment of the ZY11 publication, the properties of MHD turbulence in the relativistic regime were mostly unclear, and the possibility of extending the LV99 model to the relativistic regime was also in question. Nevertheless, ICMART (ZY11 for details) was able to successfully address a number of problems (e.g., low efficiency, electron fast cooling, electron number, and weak or no photosphere emission in some GRBs) encountered by the internal shock model (Kumar 1999; Daigne & Mochkovitch 1998; Ghisellini et al. 2000).

Since the publication of ZY11, the theoretical foundations of the GRB model based on turbulent reconnection, in particular, the LV99 model, have been strengthened (see Lazarian et al. 2016 for a review). This includes a better theoretical understanding of turbulent reconnection (see Eyink et al. 2011, Eyink 2015), more numerical testing (Kowal et al. 2012b, 2017; Eyink et al. 2013; Oishi et al. 2015; Beresnyak 2017), and more observational evidence (e.g., Lalescu et al. 2015). Most importantly, the theory of relativistic MHD turbulence has been advanced (see Takamoto & Lazarian 2016, 2017), and the relativistic turbulent reconnection has been demonstrated numerically in TIL15 and Takamoto (2018). These updates made it important to revisit the ICMART model.

On the other hand, from the observational front, many new observations since ZY11 support the general picture of the ICMART model at least in some (probably in most) GRBs. These include the polarized γ-ray and optical emission of GRB prompt emission and early afterglow (Yonetoku et al. 2011, 2012; Mundell et al. 2013; Troja et al. 2017), the progressively tight upper limits of the neutrino flux from GRBs (Aartsen et al. 2015, 2016, 2017), as well as evidence of bulk acceleration and/or anisotropy in the GRB emission region (Uhm & Zhang 2016a, 2016b; Geng et al. 2017). This motivated us to further develop the ICMART model in terms of more robust reconnection physics and an alternative (and probably more realistic) triggering mechanism.

This paper addresses the above observational challenges by presenting and quantifying a new mechanism of triggering flares of reconnection. It appeals to the kink instability, which alters the original configuration to that prone to magnetic reconnection. The inclusion of the kink instability in the ICMART model is supported by both theoretical arguments and numerical simulations (see Singh et al. 2016). This significantly improves the ability of the model to explain observational data. A bursty emission model due to turbulent reconnection is discussed in detail in view of the latest developments in reconnection physics. This lays a solid ground for the sketchy picture delineated in the ICMART model of ZY11.

A.L. acknowledges the support of the NSF grant DMS 1622353 and AST 1715754 and thanks Misha Medvedev for

helpful discussions that initiated this work. B.Z. acknowledges NASA NNX15AK85G for support. S.X. acknowledges the support for program number HST-HF2-51400.001-A provided by NASA through a grant from the Space Telescope Science Institute, which is operated by the Association of Universities for Research in Astronomy, Incorporated, under NASA contract NAS5-26555.

Appendix
Magnetic Reconnection in Turbulence

The problem that challenges the traditional reconnection model, known as the Sweet–Parker model, is the unrealistically slow reconnection rate in astrophysical conditions. This inefficiency arises from the disparity between the astrophysical scale L_x, over which the plasma is carried into the reconnection region, and the microphysical scale Δ determined by the plasma resistivity, over which the plasma is ejected from the reconnection region. Taking into account that the ejection velocity is approximately the Alfvén velocity V_A, one can easily find that the reconnection rate for incompressible media,

$$V_{rec} \approx V_A \frac{\Delta}{L_x}, \quad (15)$$

is very low, $\ll V_A$. In fact, for the outflow region determined by the ohmic resistivity $\Delta \approx \eta/V_{rec}$, one recovers the Sweet–Parker formula for the reconnection rate $V_{rec,SP} \approx V_A S^{-1/2}$. Here $S = L_x V_A/\eta$ is the Lundquist number, where η is the resistivity. This can be huge, e.g., on the order 10^{10} or even 10^{20}, in many astrophysical situations. As a result, the reconnection rate in the classical Sweet–Parker model is negligible for typical astrophysical settings.

Here we show that the situation changes dramatically in the presence of turbulence. Turbulence is ubiquitous in astrophysical environments, and it is detected essentially in every case where it is searched for, e.g., the so-called "Big Power Law in the Sky" of interstellar electron density fluctuations (Armstrong et al. 1995; Chepurnov & Lazarian 2010) and nonthermal line width broadening of various spectral lines. As we discuss in the main text, there are strong reasons for us to expect that the reconnection in GRB environments takes place in a turbulent medium.

Turbulence is stochastic, but it obeys statistical laws. The famous Kolmogorov scaling is an example of such a law. For incompressible MHD turbulence, an analog of the Kolmogorov theory is the theory proposed in GS95 (also see Brandenburg & Lazarian 2013 for a review).[8] The GS95 theory is the basis of the LV99 theory of magnetic reconnection.

In this paper we employ the model of turbulent reconnection in LV99. This model of nonrelativistic reconnection has been numerically tested by Kowal et al. (2009, 2012b) and was successfully compared with observations in a number of studies (see Ciaravella & Raymond 2008; Sych et al. 2009; Eyink et al. 2013; Kadowaki et al. 2015; Khiali et al. 2015; Lalescu et al. 2015; see also Lazarian et al. 2015, 2016 for reviews).[9] Note that the LV99 expression that we apply has also been rederived using other theoretical approaches in Eyink et al. (2011) and Eyink (2015).

Within the LV99 model, the outflow region is determined by the magnetic field line wandering. This is in contrast to the Sweet–Parker model, where the outflow is determined by the plasma microscopic diffusivity. As a result, within the LV99 model, the reconnection can be both fast and slow depending on the level of turbulence. If turbulence is of low amplitude, the magnetic field wandering is small, and thus the resulting outflow opening Δ is strongly constrained. The reconnection speed can be obtained from the mass conservation (see Equation (15)). The outflow thickness grows as the level of turbulence increases. Naturally, this increases the rate of turbulent reconnection. The fact that the reconnection can be both slow and fast is important for explaining reconnection explosions that we claim are a part of the GRB phenomenon.

The phenomenon of wandering or meandering of the magnetic field is well known (see Jokipii 1973), analytically described (LV99) and numerically tested (see Lazarian et al. 2004; Beresnyak 2013b). This effect has been applied for decades to studying the perpendicular diffusion of cosmic rays in astrophysical magnetic fields, although the proper quantitative treatment of the effect was only developed in LV99. LV99 not only serves as a theory for the turbulent reconnection, but also provides a different physical interpretation of the GS95 theory of turbulence. In particular, one can describe turbulent motions as eddies perpendicular to the magnetic field. The induced mixing of field lines in the direction perpendicular to the magnetic field is most energetically favorable as it does not involve magnetic field bending. Such mixing motions of field lines are facilitated by the turbulent reconnection that acts within one eddy turnover time. While in the original GS95 paper, the mixing motions were believed to be in the direction perpendicular to the mean magnetic field, LV99 pointed out that it should be local magnetic field that matters. Naturally, as the perpendicular mixing is not subject to the magnetic tension, it leads to the energy cascade consistent with the Kolmogorov spectrum. As the other corner stone of the GS95 theory, the scaling relation of anisotropic MHD turbulence can also be easily understood in the LV99 picture. It is the consequence of the equalization between the period of the Alfvénic perturbation along the magnetic field and the eddy turnover time.

LV99 extended the GS95 theory to the sub-Alfvénic regime and used this extended theory to obtain the expression of Δ from magnetic field wandering,

$$\Delta \approx L_x \left(\frac{2\epsilon_{inj} l}{V_A^3}\right)^{1/2} \min\left[\left(\frac{L_x}{l}\right)^{1/2}, \left(\frac{l}{L_x}\right)^{1/2}\right], \quad (16)$$

where l and L_x are the turbulence injection scale and the length of the "current sheet," respectively, while ϵ_{inj} is turbulent energy cascading rate, which, as we discuss in the main text, must be associated with the Alfvénic component of the MHD turbulence. In turbulent media an individual "current sheet"

[8] We believe that the time of vigorous debates on whether the GS95 model should be modified, e.g., by taking into account additional effects such as alignment/polarization (Boldyrev 2005, 2006; Beresnyak & Lazarian 2006), nonlocality of turbulence (Gogoberidze 2007), is over. Both theoretical (Beresnyak & Lazarian 2010) and numerical (Beresnyak 2013a, 2014) studies suggest that the GS95 model provides a proper description of MHD turbulence. Therefore here we do not discuss alternative turbulence models. In any case, the insignificant changes of the scalings, e.g., from the Kolmogorov spectrum of $k^{-5/3}$ to the Kraichnan spectrum of $k^{-3/2}$ advocated by alternative constructions, do not significantly change the model of turbulent reconnection in our consideration.

[9] We note that in the review by Karimabadi & Lazarian (2013), it was stated that no studies revealed the correspondence between the observed solar wind reconnection and the LV99 predictions. This deficiency was corrected in Lalescu et al. (2015), where such a correspondence was found.

evolves to produce a complex network of fractal current sheets, which extends over the thickness $\sim\Delta$ determined by magnetic field line wandering. The speed of reconnection $V_{\rm rec}$ can trivially be obtained from the mass conservation condition:

$$\rho_i V_{\rm rec} L_x = \rho_s V_{\rm A} \Delta, \tag{17}$$

where ρ_i is the density of the inflow and ρ_s is the density of the matter in the "current sheet." Therefore the reconnection velocity can be expressed as

$$V_{\rm rec} \approx V_{\rm A}\left(\frac{\rho_s}{\rho_i}\right)\left(\frac{2\epsilon_{\rm inj} l}{V_{\rm A}^3}\right)^{1/2} \times \min\left[\left(\frac{L_x}{l}\right)^{1/2}, \left(\frac{l}{L_x}\right)^{1/2}\right]. \tag{18}$$

Under the incompressible approximation adopted in LV99, $\rho_s = \rho_i$, and this simplifies Equation (18).

For sub-Alfvénic driving, which is most relevant to highly magnetized environments, the injection of energy is related to the velocity at the injection scale V_l according to the expression (LV99)

$$\epsilon_{\rm inj} \approx V_l^4/2lV_{\rm A}, \tag{19}$$

which is different from the expressions of energy injection that are used in hydrodynamic turbulence. Therefore, if the turbulence at the scale l is injected at the velocity $V_{\rm inj}$, Equation (19) suggests a rather unusual relation between the velocity of injection $V_{\rm inj}$ and the velocity V_l that is established at the injection scale l. Namely, as $\epsilon_{\rm inj} \sim V_{\rm inj}^2/t_{\rm inj}$, one obtains $V_{\rm inj} \sim V_l^2$. This relation is used in the main text.

Combining Equations (18) and (19), one can obtain

$$V_{\rm rec} \approx V_{\rm A} \min\left[\left(\frac{L_x}{l}\right)^{1/2}, \left(\frac{l}{L_x}\right)^{1/2}\right]\left(\frac{V_l}{V_{\rm A}}\right)^2, \tag{20}$$

which indicates that $V_{\rm rec}$ of turbulent reconnection differs from $V_{\rm A}$ by a factor that depends on the ratio between the turbulence injection scale to the current sheet scale, as well as on the ratio of the velocity at the injection scale to the Alfvén velocity.

ORCID iDs

Bing Zhang https://orcid.org/0000-0002-9725-2524
Siyao Xu https://orcid.org/0000-0002-0458-7828

References

Aartsen, M. G., Abraham, K., Ackermann, M., et al. 2016, ApJ, 824, 115
Aartsen, M. G., Ackermann, M., Adams, J., et al. 2015, ApJL, 805, L5
Aartsen, M. G., Ackermann, M., Adams, J., et al. 2017, ApJ, 843, 112
Abdo, A. A., Ackermann, M., Ajello, M., et al. 2009b, ApJL, 706, L138
Abdo, A. A., Ackermann, M., Arimoto, M., et al. 2009a, Sci, 323, 1688
Alves, E. P., Zrake, J., & Fiuza, F. 2018, PhRvL, 121, 245101
Armstrong, J. W., Rickett, B. J., & Spangler, S. R. 1995, ApJ, 443, 209
Axelsson, M., Church, R. P., Davies, M. B., Levan, A. J., & Ryde, F. 2011, MNRAS, 412, 2260
Band, D., Matteson, J., Ford, L., et al. 1993, ApJ, 413, 281
Bárta, M., Büchner, J., Karlický, M., & Skála, J. 2011, ApJ, 737, 24
Baty, H. 2001, A&A, 367, 321
Baty, H., & Heyvaerts, J. 1996, A&A, 308, 935
Beckwith, K., & Stone, J. M. 2011, ApJS, 193, 6
Beniamini, P., & Giannios, D. 2017, MNRAS, 468, 3203
Beresnyak, A. 2013a, arXiv:1301.7425
Beresnyak, A. 2013b, ApJL, 767, L39
Beresnyak, A. 2014, arXiv:1410.0957
Beresnyak, A. 2017, ApJ, 834, 47
Beresnyak, A., & Lazarian, A. 2006, ApJL, 640, L175
Beresnyak, A., & Lazarian, A. 2010, ApJL, 722, L110
Bhattacharjee, A., Huang, Y.-M., Yang, H., & Rogers, B. 2009, PhPl, 16, 112102
Biskamp, D. 1986, PhFl, 29, 1520
Bisnovatyi-Kogan, G. S., & Lovelace, R. V. E. 2001, NewAR, 45, 663
Blandford, R. D., & Payne, D. G. 1982, MNRAS, 199, 883
Blandford, R. D., & Znajek, R. L. 1977, MNRAS, 179, 433
Boldyrev, S. 2005, ApJL, 626, L37
Boldyrev, S. 2006, PhRvL, 96, 115002
Brandenburg, A., & Lazarian, A. 2013, SSRv, 178, 163
Burgess, J. M., Bégué, D., Bacelj, A., et al. 2018, arXiv:1810.06965
Cassak, P. A., Shay, M. A., & Drake, J. F. 2009, PhPl, 16, 120702
Chepurnov, A., & Lazarian, A. 2010, ApJ, 1710, 853
Ciaravella, A., & Raymond, J. C. 2008, ApJ, 686, 1372
Daigne, F., & Mochkovitch, R. 1998, MNRAS, 296, 275
Cho, J. 2005, ApJ, 621, 324
Cho, J., & Lazarian, A. 2002, PhRvL, 88, 245001
Cho, J., & Lazarian, A. 2003, MNRAS, 345, 325
Coburn, W., & Boggs, S. E. 2003, Natur, 423, 415
Daughton, W., Nakamura, T. K. M., Karimabadi, H., Roytershteyn, V., & Loring, B. 2014, PhPl, 21, 052307
Daughton, W., Roytershteyn, V., Albright, B. J., et al. 2009, PhRvL, 103, 065004
Daughton, W., Roytershteyn, V., Karimabadi, H., et al. 2011, NatPh, 7, 539
Daughton, W., Scudder, J., & Karimabadi, H. 2006, PhPl, 13, 072101
Deng, W., Li, H., Zhang, B., & Li, S. 2015, ApJ, 805, 163
Drake, J. F. 2001, in APS Meeting Abstract 46, April Meeting (Riverdale, MD: APS)
Drake, J. F., Swisdak, M., Che, H., & Shay, M. A. 2006, Natur, 443, 553
Drenkhahn, G., & Spruit, H. C. 2002, A&A, 391, 1141
Eyink, G. L. 2010, PhRvE, 82, 046314
Eyink, G. L. 2015, ApJ, 807, 137
Eyink, G. L., Lazarian, A., & Vishniac, E. T. 2011, ApJ, 743, 51, (ELV11)
Eyink, G., Vishniac, E., Lalescu, C., et al. 2013, Natur, 497, 466
Fermo, R. L., Drake, J. F., & Swisdak, M. 2012, PhRvL, 108, 255005
Galsgaard, K., & Nordlund, Å. 1997, JGR, 102, 219
Gao, H., & Zhang, B. 2015, ApJ, 801, 103
Gao, H., Zhang, B.-B., & Zhang, B. 2012, ApJ, 748, 134
Garrison, D., & Nguyen, P. 2016, JMPh, 7, 281
Geng, J.-J., Huang, Y.-F., & Dai, Z.-G. 2017, ApJL, 841, L15
Geng, J.-J., Huang, Y.-F., Wu, X.-F., Zhang, B., & Zong, H-S. 2018, ApJS, 234, 3
Gerrard, C. L., Arber, T. D., & Hood, A. W. 2002, A&A, 387, 687
Gerrard, C. L., & Hood, A. W. 2003, SoPh, 214, 151
Ghisellini, G., Celotti, A., & Lazzati, D. 2000, MNRAS, 313, L1
Giannios, D. 2006, A&A, 457, 763
Giannios, D. 2008, A&A, 480, 305
Giannios, D., & Spruit, H. C. 2006, A&A, 450, 887
Giannios, D., Uzdensky, D. A., & Begelman, M. C. 2009, MNRAS, 395, L29
Goedbloed, J. P. H., & Poedts, S. 2004, Principles of Magnetohydrodynamics (Cambridge: Cambridge Univ. Press)
Gogoberidze, G. 2007, PhPl, 14, 022304
Goldreich, P., & Sridhar, S. 1995, ApJ, 438, 763
Goodman, J. 1986, ApJL, 308, L47
Guiriec, S., Briggs, M. S., & Connaugthon, V. 2010, ApJ, 725, 225
Gutiérrez, H., Taliashvili, L., Lazarian, A., & Mouradian, Z. 2017, MNRAS, 471, 4776
Huang, Y.-M., & Bhattacharjee, A. 2010, PhPl, 17, 062104
Huang, Y.-M., & Bhattacharjee, A. 2012, PhRvL, 109, 265002
Huang, Y.-M., & Bhattacharjee, A. 2013, PhPl, 20, 055702
Huang, Y.-M., & Bhattacharjee, A. 2016, ApJ, 818, 20
Huang, Y.-M., Bhattacharjee, A., & Sullivan, B. P. 2011, PhPl, 18, 072109
Inoue, T., Asano, K., & Ioka, K. 2011, ApJ, 734, 77
Jafari, A., Vishniac, E. T., Kowal, G., & Lazarian, A. 2018, ApJ, 860, 52
Jia, L.-W., Uhm, Z. L., & Zhang, B. 2016, ApJS, 225, 17
Jokipii, J. R. 1973, ApJ, 183, 1029
Kadowaki, L. H. S., de Gouveia Dal Pino, E. M., & Singh, C. B. 2015, ApJ, 802, 113
Karimabadi, H., & Lazarian, A. 2013, PhPl, 20, 112102
Kato, S., Fukue, J., & Mineshige, S. 2008, Black-Hole Accretion Disks: Toward a New Paradigm (2nd ed.; Kyoto: Kyoto Univ. Press)

Khiali, B., de Gouveia Dal Pino, E. M., & del Valle, M. V. 2015, MNRAS, 449, 34
Kobayashi, S., Piran, T., & Sari, R. 1997, ApJ, 490, 92
Kowal, G., de Gouveia Dal Pino, E., & Lazarian, A. 2012a, PhRvL, 108, 241102
Kowal, G., Falceta-Gonçalves, D. A., Lazarian, A., & Vishniac, E. T. 2017, ApJ, 838, 91
Kowal, G., & Lazarian, A. 2010, ApJ, 720, 742
Kowal, G., Lazarian, A., Vishniac, E. T., & Otmianowska-Mazur, K. 2009, ApJ, 700, 63
Kowal, G., Lazarian, A., Vishniac, E. T., & Otmianowska-Mazur, K. 2012b, NPGeo, 19, 297
Kumar, P. 1999, ApJL, 523, L113
Kumar, P., & McMahon, E. 2008, MNRAS, 384, 33
Kumar, P., & Zhang, B. 2015, PhR, 561, 1
Lalescu, C. C., Shi, Y.-K., Eyink, G. L., et al. 2015, PhRvL, 115, 025001
Lapenta, G. 2008, PhRvL, 100, 235001
Lapenta, G., & Lazarian, A. 2012, NPGeo, 19, 251
Lazarian, A., Eyink, G., Vishniac, E., & Kowal, G. 2015, RSPTA, 373, 20140144
Lazarian, A., Kowal, G., Takamoto, M., de Gouveia Dal Pino, E. M., & Cho, J. 2016, ASSL, 427, 409
Lazarian, A., Petrosian, V., Yan, H., & Cho, J. 2003, arXiv:astro-ph/0301181
Lazarian, A., & Vishniac, E. 1999, ApJ, 517, 700, (LV99)
Lazarian, A., Vishniac, E., & Cho, J. 2004, ApJ, 603, 180
Lazarian, A., & Vishniac, E. T. 2009, RMxAC, 36, 81
Lazzati, D., & Begelman, M. C. 2010, ApJ, 725, 1137
Li, L.-X. 2000, ApJL, 531, L111
Lithwick, Y., & Goldreich, P. 2001, ApJ, 562, 279
Lithwick, Y., & Sari, R. 2001, ApJ, 555, 540
Loureiro, N. F., Schekochihin, A. A., & Cowley, S. C. 2007, PhPl, 14, 100703
Lu, R.-J., Wei, J. J., Liang, E. W., et al. 2012, ApJ, 756, 112
Lyutikov, M. 2003, MNRAS, 346, 540
Lyutikov, M., & Blandford, R. 2003, arXiv:astro-ph/0312347
Lyutikov, M., & Lazarian, A. 2013, SSR, 178, 459
Lyutikov, M., & Uzdensky, D. 2003, ApJ, 589, 893
Lyubarsky, Y. E. 2005, MNRAS, 358, 113
McKinney, J. C., & Blandford, R. D. 2009, MNRAS, 394, L126
McKinney, J. C., & Uzdensky, D. A. 2012, MNRAS, 419, 573
Mészáros, P., & Rees, M. J. 1993, ApJ, 405, 278
Mészáros, P., & Rees, M. J. 1997, ApJ, 476, 232
Mészáros, P., & Rees, M. J. 2000, ApJ, 530, 292
Mignone, A., Tzeferacos, P., & Bodo, G. 2010, JCoPh, 229, 5879
Mizuno, Y., Hardee, P. E., & Nishikawa, K.-I. 2011a, ApJ, 734, 19
Mizuno, Y., Hardee, P. E., & Nishikawa, K.-I. 2014a, ApJ, 784, 167
Mizuno, Y., Lyubarsky, Y., Nishikawa, K.-I., & Hardee, P. E. 2009, ApJ, 700, 684
Mizuno, Y., Lyubarsky, Y., Nishikawa, K.-I., & Hardee, P. E. 2012, ApJ, 757, 16
Mizuno, Y., Pohl, M., Niemiec, J., et al. 2011b, ApJ, 726, 62
Mizuno, Y., Pohl, M., Niemiec, J., et al. 2014b, MNRAS, 439, 3490
Mundell, C. G., Kopac, D., Arnold, D. M., et al. 2013, Natur, 504, 119
Nava, L., Ghirlanda, G., Ghisellini, G., & Celotti, A. 2011, A&A, 530, A21
Norris, J. P., Bonnell, J. T., Kazanas, D., et al. 2005, ApJ, 627, 324
Norris, J. P., Marani, G. F., & Bonnell, J. T. 2000, ApJ, 534, 248
O'Neill, S. M., Beckwith, K., & Begelman, M. C. 2012, MNRAS, 422, 1436
Oishi, J. S., Mac Low, M.-M., Collins, D. C., & Tamura, M. 2015, ApJL, 806, L12
Paczýnski, B. 1986, ApJL, 308, L43
Pe'er, A., Zhang, B. B., Ryde, F., et al. 2012, MNRAS, 420, 468
Petschek, H. E. 1964, in Magnetic field annihilation. The Physics of Solar Flares, AAS-NASA Symp. (NASA SP-50), ed. W. H. Hess (Greenbelt, MD: NASA), 425
Preece, R. D., Briggs, M. S., Mallozzi, R. S., et al. 2000, ApJS, 126, 19
Rees, M. J., & Mészáros, P. 1992, MNRAS, 258, 41P
Rees, M. J., & Mészáros, P. 1994, ApJL, 430, L93
Ryde, F., Axelsson, M., Zhang, B. B., et al. 2010, ApJL, 709, L172
Shay, M. A., Drake, J. F., Denton, R. E., & Biskamp, D. 1998, JGR, 103, 9165
Shemi, A., & Piran, T. 1990, ApJL, 365, L55
Shen, C., Lin, J., & Murphy, N. A. 2011, ApJ, 737, 14
Shepherd, L. S., & Cassak, P. A. 2010, PhRvL, 105, 015004
Shibata, K., & Tanuma, S. 2001, EP&S, 53, 473
Singh, C. B., Mizuno, Y., & de Gouveia Dal Pino, E. M. 2016, ApJ, 824, 48
Somov, B. V., & Verneta, A. I. 1993, SSRv, 65, 253
Spruit, H. C., Daigne, F., & Drenkhahn, G. 2001, A&A, 369, 694
Steele, I. A., Mundell, C. G., Smith, R. J., Kobayashi, S., Guidorzi, C., et al. 2009, Natur, 462, 767
Sych, R., Karlický, M., Altyntsev, A., Dudík, J., & Kashapova, L. 2015, A&A, 577, A43
Sych, R., Nakariakov, V. M., Karlicky, M., & Anfinogentov, S. 2009, A&A, 505, 791
Syrovatskii, S. I. 1981, ARA&A, 19, 163
Takamoto, M. 2013, ApJ, 775, 50
Takamoto, M. 2018, MNRAS, 476, 4263
Takamoto, M., Inoue, T., & Lazarian, A. 2015, ApJ, 815, 16
Takamoto, M., & Lazarian, A. 2016, ApJL, 831, L11
Takamoto, M., & Lazarian, A. 2017, MNRAS, 472, 4542
Taylor, G. B., Frail, D. A., Berger, E., & Kulkarni, S. R. 2004, ApJL, 609, L1
Thompson, C. 1994, MNRAS, 270, 480
Thompson, C., & Blaes, O. 1998, PhRvD, 57, 3219
Tomimatsu, A., Matsuoka, T., & Takahashi, M. 2001, PhRvD, 64, 123003
Török, T., Kliem, B., & Titov, V. S. 2004, A&A, 413, L27
Troja, E., Piro, L., van Eerten, H., et al. 2017, Natur, 551, 71
Uhm, Z. L., & Zhang, B. 2014, NatPh, 10, 351
Uhm, Z. L., & Zhang, B. 2016a, ApJ, 825, 97
Uhm, Z. L., & Zhang, B. 2016b, ApJL, 824, L16
Uhm, Z. L., Zhang, B., & Racusin, J. L. 2018, ApJ, 869, 100
Usov, V. V. 1992, Natur, 357, 472
Uzdensky, D. A., Loureiro, N. F., & Schekochihin, A. A. 2010, PhRvL, 105, 235002
Veres, P., Zhang, B.-B., & Mészáros, P. 2013, ApJ, 764, 94
Wiersema, K., Covino, S., & Toma, K. 2014, Natur, 509, 201
Willis, D. R., Barlow, E. J., Bird, A. J., et al. 2005, A&A, 439, 245
Wyper, P. F., & Pontin, D. I. 2014, PhPl, 21, 082114
Xu, S., & Li, Z. 2014, RAA, 14, 411
Xu, S., Yang, Y.-P., & Zhang, B. 2018, ApJ, 853, 43
Xu, S., & Zhang, B. 2017, ApJL, 846, L28
Yonetoku, D., Murakami, T., Gunji, S., et al. 2011, ApJL, 743, L30
Yonetoku, D., Murakami, T., Gunji, S., et al. 2012, ApJL, 758, L1
Zhang, B. 2018, The Physics of Gamma-Ray Bursts (Cambridge: Cambridge Univ. Press)
Zhang, B., Fan, Y. Z., Dyks, J., et al. 2006, ApJ, 642, 354
Zhang, B., & Kumar, P. 2013, PhRvL, 110, 121101
Zhang, B., & Pe'er, A. 2009, ApJL, 700, L65
Zhang, B., & Yan, H. 2011, ApJ, 726, 90
Zhang, B., & Zhang, B. 2014, ApJ, 782, 92
Zhang, B., Zhang, B. B., Virgil, F. J., et al. 2009, ApJ, 703, 1696
Zhang, B.-B., Uhm, Z. L., Connaughton, V., Briggs, M. S., Zhang, B., et al. 2016, ApJ, 816, 72
Zhang, B.-B., Zhang, B., Castro-Tirado, A. J., et al. 2018, NatAs, 2, 69
Zhang, B.-B., Zhang, B., Liang, E. W., et al. 2011, ApJ, 730, 141
Zhang, S.-N., Kole, M., Bao, T. W., et al. 2019, NatAs, 3, 258
Zrake, J. 2016, ApJ, 823, 39
Zrake, J., & MacFadyen, A. I. 2012, ApJ, 744, 32
Zrake, J., & MacFadyen, A. I. 2013, ApJL, 763, L12